Paper

Investigation of the surface degradation of $LiCoO_2$ particles in the cathode materials of Li-ion batteries using FIB-TOF-SIMS

M. Ohnishi,[1#] O. Matsuoka,[2] H. Nogi[2] and T. Sakamoto[1*]

[1]*Department of Electrical Engineering, Faculty of Engineering, Kogakuin University, 2665-1 Nakano-machi, Hachiouji, Tokyo 192-0015, Japan*

[2]*Mitsui Chemicals, Inc., 580-32 Nagaura, Sodegaura, Chiba 299-0265, Japan*

(#present address: Department of Applied Chemistry Faculty of Science, Tokyo University of Science, 1-3 Kagurazaka, Shinjuku-ku, Tokyo 162-8601, Japan)

**ct13087@ns.kogakuin.ac.jp*

(Received: March 29, 2013; Accepted: October 20, 2013)

Lithium-ion batteries will be increasingly important in next-generation energy-storage devices. However, the charge-discharge mechanism of the electrode in these batteries has not yet been revealed. It has been reported that the surface crystal structure changes when these batteries degrade, but the phase transition that occurs on the surface of the cathode material has not yet been clarified because observation of the surface of the grains is insufficient. On the other hand, it has been shown that using Ga^+ primary ion time-of-flight secondary ion mass spectrometry (TOF-SIMS), a regularity can be observed in the fragment patterns of metal compounds that can provide information on their oxidation states and electron affinities. Therefore, in this study the spectra of various cobalt components, including $LiCoO_2$, CoO, and Co_3O_4 were compared, and depth profile analyses of Li-ion battery's cathode materials were conducted using a laboratory-made TOF-SIMS apparatus. Variation in the secondary ion mass spectra was observed from the surface to the interior. Although a phase transition was not directly observed via cross-sectional analysis, it was concluded that the surface of the cathode materials comprised of CoO and/or Co_3O_4, while the interior of the cathode consisted of $LiCoO_2$. Moreover, it was determined that the thickness of the CoO and/or Co_3O_4 layers on the cathode materials was less than 200 nm.

1. Introduction

Lithium-ion (Li-ion) batteries will have significant application in next-generation clean energy storage devices for natural power sources. Moreover, recent progress in the development of both pure electric vehicles and hybrid electric vehicles has resulted in higher requirements for both high power operation and long battery life. The electric power characteristics of battery systems are related to the nature of the electrode reactions. Therefore, to increase performance an understanding of the reactions at the electrodes and the various causes for electrode degradation is required. In Li-ion batteries, reactions at the electrodes include lithium diffusion within and on the cathode surface, de-solvation of lithium, and intercalation of lithium in the anode. The causes of degradation are considered to be the deposition of Li on the electrode, decomposition of the electrolyte, elution of the active material, formation of an inactive film on the electrode [1], and a phase transition of the electrode [2]. However, the actual details of the degradation mechanism are unknown.

On the other hand, it has been reported that the interface reaction between an ideal epitaxial electrode and an electrolyte depends on the orientation of the electrode [3].

In Li-ion batteries, the horizontal faces of the *c*-axis of the $LiCoO_2$ particles are electrically active. However, the details of the mechanism of the charge-discharge system for the actual material are also unknown. Thus, to develop a high-power Li-ion battery system it is essential to understand the details of the interface reaction between the electrolyte and the electrode. It is considered that $LiCoO_2$ is transformed into CoO and Co_3O_4 during charge-discharge cycles [4, 5]. To evaluate the degradation mechanisms occurring in Li-ion batteries, it is important to distinguish the surface composition of the cathode materials. Therefore, in this study we focused our attention on the phase transition of the positive electrode.

Using Ga^+ primary ion time-of-flight secondary ion mass spectrometry (TOF-SIMS), it has been shown that a certain regularity of the fragment pattern can be observed for metal compounds. This regularity of the fragment ion pattern provides chemical information, such as the oxidation state and electron affinity of the metallic elements [6-8]. Therefore, different cobalt compounds should have different secondary ion mass spectra. Thus, to visualize the composition of Li-ion cathode materials, we attempted to distinguish the different cobalt compounds present in Li-ion battery cathodes using focused ion beam (FIB)-TOF-SIMS. The secondary ion mass spectra of these individual reagents were compared to establish references for the study degradation of Li-ion batteries, and their secondary ion mass spectra were compared to those of actual cathode materials.

2. Experimental

2.1 Reagents

Control samples, including $LiCoO_2$ (99.8% trace metals basis, powder), CoO (99.99% trace metals basis, powder), and Co_3O_4 (no described degree of purity, powder), were purchased from Sigma Aldrich. Each powdered reagent was embedded on an indium substrate. The spatial resolution of $LiCoO_2$, CoO,, and Co_3O_4 was approximately 400 nm, 160 nm, and 80 nm, respectively, and corresponded to the grain size of each reagent. These spatial resolutions depended the grain size of each regent.

2.2 Cathode materials.

Positive electrodes consisting mainly of $LiCoO_2$ particles were used. Polyvinylidene difluoride and acetylene black were added as the binder and conductive material, respectively. The sample comprised of electrode particles subjected to aging in the electrolyte is referred to as the aged cathode. The electrolyte consisted of a solvent (a mixture of ethylene carbonate, ethyl methyl carbonate, and dimethyl carbonate (DMC) with a ratio of 1:1:1 vol %) and $LiPF_6$ (1 mol/l). The aging test was performed for two days at a constant temperature of 80°C under a full state-of-charge (4.2 V). After the aging test, the battery was disassembled and the positive electrode was cleaned with DMC in an inert Ar atmosphere. The cathode powder material was stripped from the electrode and embedded on an indium substrate in an air atmosphere. In general, cathode material of Li-ion battery that which is not full charge is stable than anode material. Because of the standard electrode potential (E_0) of $LiCoO_2$ is ~0.9 V [9]. The value indicates that $LiCoO_2$ is more stable than Ag, more unstable than Pt in acid solution. Thus, the influence of the atmosphere of the drying room on the $LiCoO_2$ was insignificant during the handling of the sample.

Cathode materials only soaked in the electrolyte (no aging) and before soaking in the electrolyte (no soak) were prepared as control samples.

2.3 FIB milling

The cathode materials were milled using a FIB connected to a TOF-SIMS apparatus to observe their cross-sections. The Ga^+ FIB current was set at approximately 300 pA. The rastered area was ~ 2×5 μm^2 for 10-20 min.

2.4 Surface analyses

Surface observation and chemical species mapping of the Li-ion battery cathode materials and individual reagents were performed using a TOF-SIMS apparatus [10]. The apparatus had two beams: a focused ion beam (FIB) and an electron beam (EB). In this study, the electron beam induced secondary electron images (SEM) and ion beam induced secondary electron images (SIM) and elemental maps of the cathode material and reagent particles on indium substrates were observed using a combination of pulsed FIB and TOF-SIMS. The Ga^+ FIB at an energy of 30 keV was rastered over the surface to obtain the SIM images. The beam current of the FIB was approximately 300 pA. Pulsed FIB was used as the primary ion beam for elemental mapping. Under these analytical conditions, the beam diameter was considered to be ~ several tens of nm. The pulse width was 300 ns, and the number of shots per pixel was 300 and 400 for the negative and the positive analysis modes, respectively.

2.5 Depth analyses

Depth analyses of the cathode materials were performed using the following steps (Fig. 1): secondary ion mapping analysis on the surface (primary), sputtering of the surface (~ 30 nm), secondary ion mapping (after sputter 1), deep sputtering of an ~ 3 × 3 μm^2 area (~ 60 nm), secondary ion mapping (after sputter 2). The mapping area was ~ 10 × 10 μm^2 and consisted of 128 × 128 pixels. The remaining conditions for the TOF and FIB depth analyses were the same as those used in the surface analysis mode.

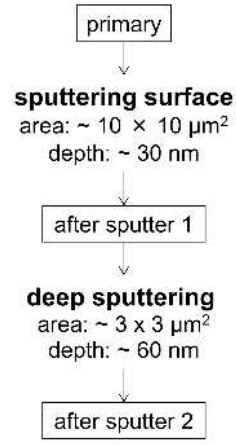

Fig. 1 Steps involved in the depth analysis

3. Results and Discussion

3.1 Reagents

Figure 2 shows the secondary ion mass spectra of pure $LiCoO_2$, CoO, and Co_3O_4. The contaminants, Na, K, F, and Cl were detected in all of the reagents. These contaminations are distributed on the reagent grains as spot and on the indium substrate. In $LiCoO_2$, $^7Li^+$ were detected. As expected, $^{59}Co^+$ were detected in all of the

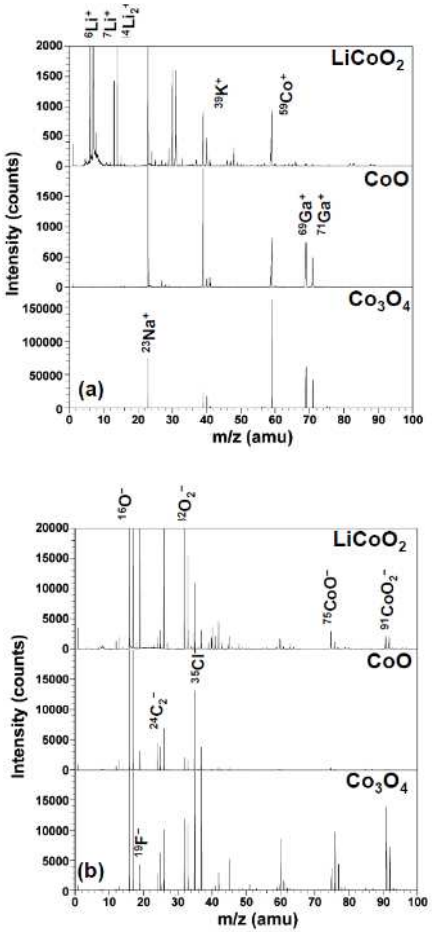

Fig. 2 Secondary ion spectra of $LiCoO_2$, CoO, and Co_3O_4. (a) Positive secondary ion spectra. (b) Negative secondary ion spectra.

samples. However, $^{75}CoO^-$ and $^{91}CoO_2^-$ were not detected in the CoO, but were observed in the $LiCoO_2$ and Co_3O_4 compounds. Moreover, the $^{75}CoO^-$ and $^{91}CoO_2^-$ content was higher in the Co_3O_4 sample than in the $LiCoO_2$ sample. Furthermore, the $^{59}Co^+/^{91}CoO_2^-$ peak intensity ratio was the highest for the CoO grains. Finally, it was determined from these spectra that the total secondary ion intensity of the Co_3O_4 sample was the highest for all of these reagents.

Figure 3 shows the SIM and secondary ion images for $^{59}Co^+$, $^{75}CoO^-$, and $^{91}CoO_2^-$. The rastered area of $LiCoO_2$, CoO, and Co_3O_4 is 50×50 μm^2, 20×20 μm^2, and 10×10 μm^2, respectively, and the number of pixel is 128 × 128. The size of $LiCoO_2$ grains was 5-20 μm, $^{75}CoO^-$ and $^{91}CoO_2^-$ were distributed over the entire surfaces of these grains, and few $^{59}Co^+$ were emitted from them.

On the other hand, most of the CoO grains were smaller than 5 μm had clear crystal faces, and adopted a nearly subhedral shape. Moreover, each CoO grain was attached to other grains, and $^{59}Co^+$ were strongly detected from the upper edges of the grains, while the $^{75}CoO^-$ and $^{91}CoO_2^-$ ions were less intense.

Finally, the size of the Co_3O_4 grains was approximately 5 μm, and these crystals also adopted a subhedral shape. However, unlike CoO, $^{59}Co^+$ were detected at the upper faces of the grains, and $^{75}CoO^-$ and $^{91}CoO_2^-$ were detected over the entire crystal face.

Table 1 presents the maximum counts for each secondary ion per pixel in Fig. 3. Many more $^{75}CoO^-$ and $^{91}CoO_2^-$ than $^{59}Co^+$ were detected from $LiCoO_2$, while many $^{59}Co^+$ were detected from CoO. On the other hand, $^{59}Co^+$, $^{75}CoO^-$, and $^{91}CoO_2^-$ were detected from the Co_3O_4. The results of the secondary ion mapping also indicate that the secondary ions of Co_3O_4 are more intense than those of the other reagents.

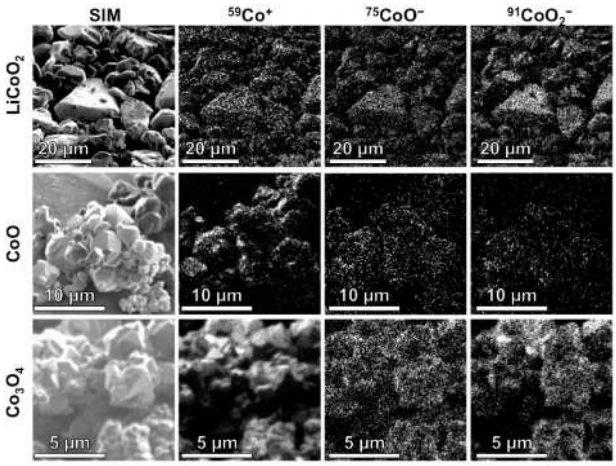

Fig. 3 FIB-induced secondary electron image (SIM) and secondary ion maps for $LiCoO_2$, CoO, and Co_3O_4.

Table 1 Maximum counts for each secondary ion per pixel in Fig. 3.

	$LiCoO_2$	CoO	Co_3O_4
$^{59}Co^+$	8	131	235
$^{91}CoO_2^-$	14	3	26
$^{75}CoO^-$	12	6	9

3.2 Mixture of reagents

Figure 4 shows the secondary ion mapping of a mixture of $LiCoO_2$, CoO, and Co_3O_4. The rastered area of these images are 30 × 30 μm^2, and the number of pixel is 128 × 128. The distribution of $^7Li^+$ indicated the presence of $LiCoO_2$ grains, while intense $^{59}Co^+$ signals indicated

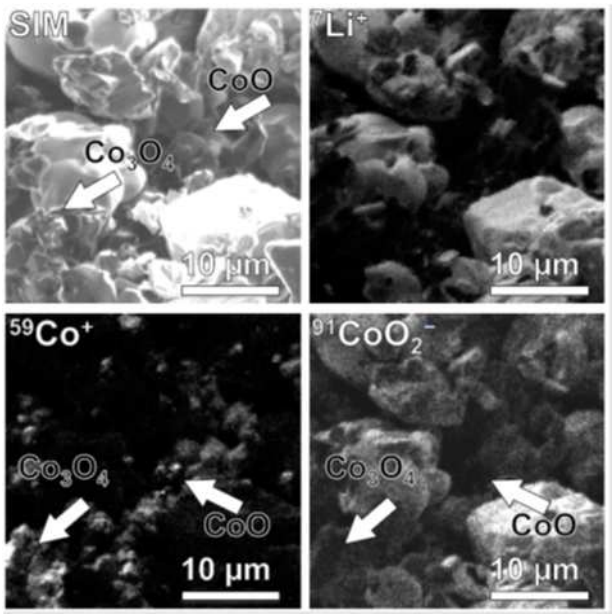

Fig. 4 FIB-induced secondary electron image (SIM) and secondary ion maps for a mixture of $LiCoO_2$, CoO, and Co_3O_4.

the CoO and Co_3O_4 grains. In contrast, the $^{75}CoO^-$ and $^{91}CoO_2^-$ signals denoted the locations of the $LiCoO_2$ and Co_3O_4 grains. These results confirmed that $^{59}Co^+$ was strongly detected from CoO and Co_3O_4, but not from $LiCoO_2$. Moreover, because $^{75}CoO^-$ and $^{91}CoO_2^-$ were only detected for $LiCoO_2$ and Co_3O_4, and the $^7Li^+$ signal was only intense for $LiCoO_2$, it was possible to distinguish the cobalt components in the mixture using secondary ion mass spectroscopy.

These tendencies are well explained by the bond-breaking model [11]. Secondary ions of Co^+ and O^- are emitted by the covalent bond breaking of CoO. Moreover, Co_3O_4 is a mixed-valence compound consisting of CoO and Co_2O_3. Thus, it emits Co^+ and O^- by cleavage of the CoO bond. Similarly, O^-, CoO^-, CoO^+, CoO_2^-, CoO_2^+, and $Co_2O_2^+$ are formed by cleavage of the Co_2O_3 bonds. On the other hand, ionic bonds were preferentially broken in the case of $LiCoO_2$. Thus, $^{75}CoO^-$ and $^{91}CoO_2^-$ were more easily emitted than $^{59}Co^+$ from $LiCoO_2$.

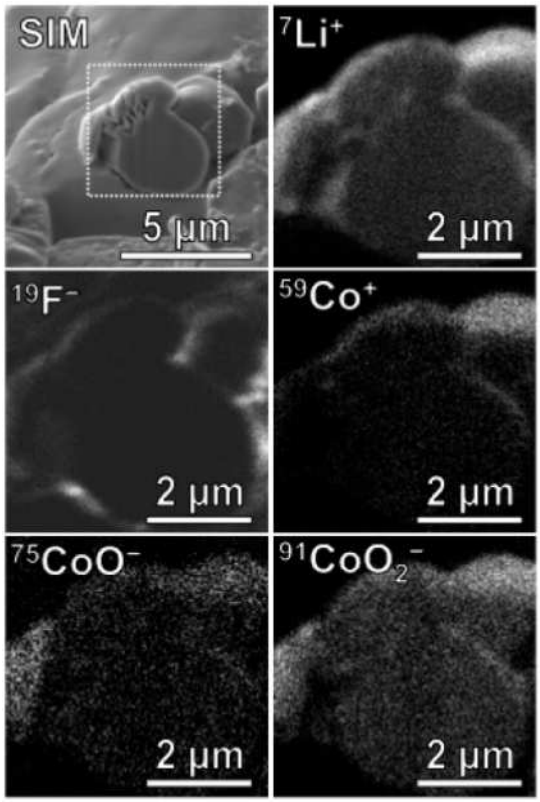

Fig. 5 FIB-induced secondary electron image (SIM) and secondary ion maps for the cross-sectional analysis. The rectangle indicates the mapping area.

3.3 The cathode materials

The results of the mapping of the cross section of the aged cathode using FIB is shown in Fig. 5. The rastered area of these images are 5×5 μm^2, and the number of pixel is 128×128. In the figure, it can be seen that $^{19}F^-$ was present only on the surface of the grains. Hence, it can be considered that $^{19}F^-$ cannot diffuse into the interior of the cathode materials. Figure 6 presents the line profiles of the $^{59}Co^+$ counts and intensities in the SIM image in Fig. 5.

These line profiles were obtained by summing 4 pixels in the vertical direction in the images. The intensity of the SIM image is enhanced near the grains (edge effect), and the $^{59}Co^+$ count and the intensity of the SIM image follow the same trend. Moreover, it is difficult to distinguish the distribution of $^{59}Co^+$ and the edge effect. In fact, under these conditions the edge effect was estimated to be approximately 200 nm, and the edge effect and the

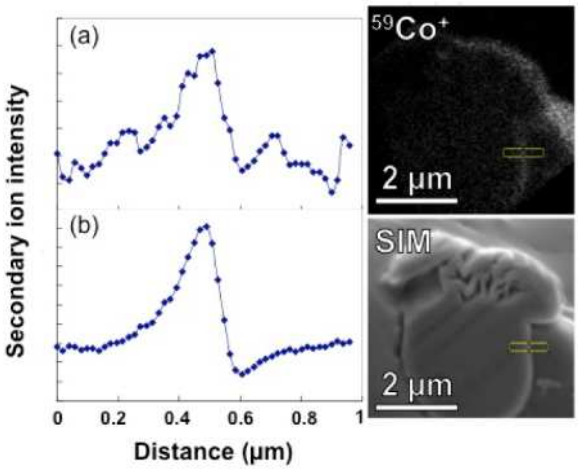

Fig. 6 Line profiles of the (a) $^{59}Co^+$ counts and (b) intensity of the SIM image in Fig. 5. These line profiles were obtained by summing 4 pixels in the vertical direction in the images.

distribution of $^7Li^+$, $^{59}Co^+$, $^{75}CoO^-$, and $^{91}CoO_2$- cannot be clarified. Therefore, these results indicate that the distribution of $^7Li^+$, $^{59}Co^+$, $^{75}CoO^-$, and $^{91}CoO_2^-$ in the aged cathode was less than 200 nm. It can also be seen that the

$^{7}Li^{+}$, $^{59}Co^{+}$, $^{75}CoO^{-}$, and $^{91}CoO_2^{-}$ are homogeneously distributed throughout the interior of the cathode material.

Figure 7 presents the secondary ion mapping results for the no soak cathode. The rastered area of these images are 10×10 μm^2, and the number of pixel is 128×128. The intensity of the $^{75}CoO^{-}$ and $^{91}CoO_2^{-}$ is higher than that of $^{59}Co^{+}$, indicating that the no soak cathode is similar to $LiCoO_2$.

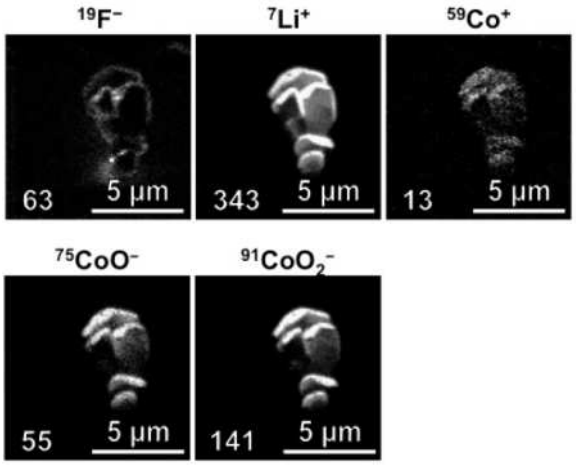

Fig. 7 Secondary ion maps of the no soak cathode. The numbers in the bottom-left corner of each image are the maximum counts for the secondary ion intensities.

The depth analysis of the no aging cathode is shown in Fig. 8. Most of the counts for $^{19}F^{-}$ were once again on the surface of the cathode. The $^{19}F^{-}$ is assumed to originate from the electrolyte. Moreover, there was little difference in the intensities of the $^{7}Li^{+}$ on the surface and in the interior, which indicates that only a minor amount of lithium fluoride was produced via reaction with the HF generated upon hydrolysis of $LiPF_6$ [1] and also confirms that the effect of exposure to the atmosphere was small.

However, the $^{91}CoO_2^{-}/^{59}Co^{+}$ on the surface of the no aging cathode was higher than that in the interior. This result indicates that the surface of the no aging cathode was altered by just soaking in the electrolyte. This result is consistent with a previous study [12], which found that the surface Co ions were extracted from a cathode soaked in electrolyte.

The depth analysis results for the aged cathode are

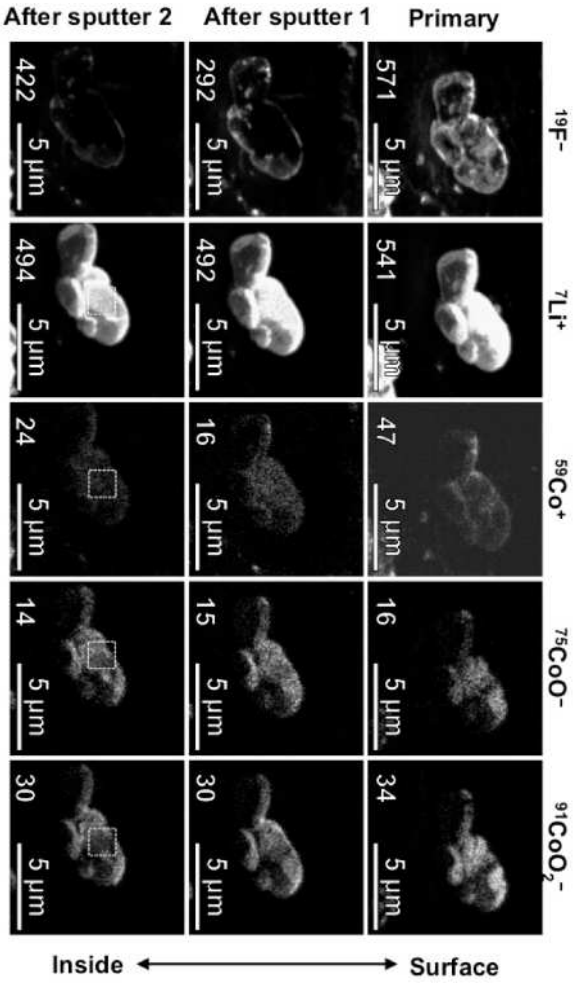

Fig. 8 Secondary ion maps of the no aging cathode. The numbers in the bottom-left corner of each image are the maximum counts for the secondary ion intensities. The rectangles indicate the deep sputtering areas.

shown in Fig. 9. The $^{7}Li^{+}$ counts were largest on the surface. It initially decreased as the sputtering depth increased, and then eventually increased. The highest intensity for $^{7}Li^{+}$ on the surface corresponds with the behavior of the $^{19}F^{-}$ intensity. These results suggest that lithium fluoride, which is produced during the charge-discharge cycles, affected the intensity of the $^{7}Li^{+}$ on the surface.

On the other hand, because the intensity of the $^{7}Li^{+}$ is higher in the interior cathode grains, it can be concluded that the interior of the cathode material after the aging test consisted of $LiCoO_2$.

Like the $^{7}Li^{+}$, the $^{91}CoO_2^{-}/^{59}Co^{+}$ ratio increased from

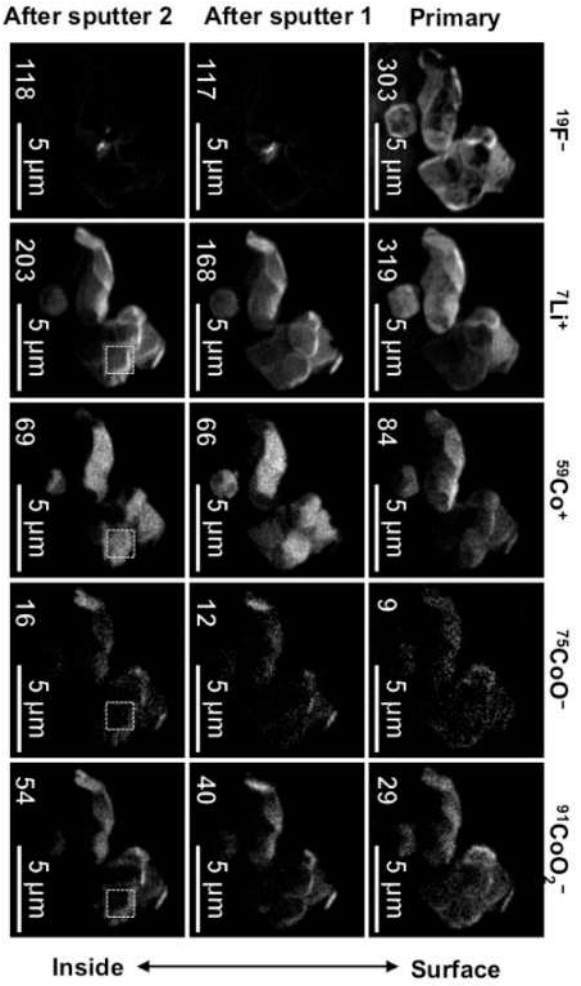

Fig. 9 Secondary ion maps of the aged cathode. The numbers in the bottom-left corner of each image are the maximum counts for the secondary ion intensities. The rectangles indicate the deep sputtering areas.

the surface to the interior. This result indicates that the material on the surface of the cathode changed from the original composition, containing only a little $^{75}CoO^-$ and $^{91}CoO_2^-$ to a composition containing significantly more $^{75}CoO^-$ and $^{91}CoO_2^-$, while the interior of the cathode material remained unchanged. Thus, the aged cathode material contained CoO and/or Co_3O_4 on the surface and $LiCoO_2$ in the interior. It was also confirmed from the cross-sectional analysis that the interior of the cathode material consisted of $LiCoO_2$, because fewer $^{59}Co^+$ were detected in the interior than on the surface and larger numbers of $^{75}CoO^-$, $^{91}CoO_2^-$, and $^{7}Li^+$ ions were detected in the interior of the aged cathode material (Fig.5).

On the other hand, no clear phase transition was observed in the cross section of the aged cathode (Fig. 6), which implies that the thickness of the surface-modified region is less than 200 nm.

4. Conclusions

In this study, secondary ion spectral analysis, surface observation, and secondary ion mapping analysis of $LiCoO_2$, CoO, and Co_3O_4 were performed using a high spatial resolution FIB-TOF-SIMS apparatus. Differences in the secondary ion mass spectra of the cobalt components was demonstrated, and this information was used to evaluate the degradation of Li-ion battery cathode materials.

Moreover, the secondary ion mass spectra obtained at and near the surface of an aged cathode were different from those of the interior. Therefore, it was concluded that the $LiCoO_2$ at the surface of the cathode was converted to CoO and/or Co_3O_4, while the $LiCoO_2$ in the interior remained unchanged. Furthermore, the thickness of the surface-modified region was determined to be less than 200 nm based on a cross-sectional analysis.

5. Acknowledgment

This study was supported by SENTAN (JST).

6. References

[1] K. Edström, T. Gustafsson, J. O. Thomas, *Electrochim. Acta.* **50**, 397 (2004).

[2] J. N. Reimers and J. R. Dahn, *J. Electrochem. Soc.* **139**, 2091 (1992).

[3] M. Hirayama, N. Sonoyama, T. Abe, M. Minoura, M. Ito, D. Mori, A. Yamada, R. Kanno, T. Terashima, M. Takano, K. Tamura, J. Mizuki, *J. Power Sources* **168**, 493 (2007).

[4] D. Mohanty and H. Gabrisch, *Solid State Ionics* **194**, 41 (2011).

[5] H. Gabrisch, M. Kombolias, D. Mohanty, *Solid State Ionics* **181**, 71 (2010).

[6] Z. Li, T. Hoshi, K. Hirokawa, *Hyoumen Kagaku* **21**,

651 (2000).

[7] Z. Li and K. Hirokawa, *Analytical Sci.* **19**, 1231 (2003).

[8] R. Van Ham, A. Adriaens, L. Van Vaeck, R. Gijbels, F. Adams, *Nucl. Instrum. Methods Phys. Res.* **B 161-163**, 245 (2000).

[9] H. Izumida, *Iwate Industrial Technology Junior College bulletin* **13**, 32 (2013).

[10] T. Sakamoto, M. Koizumi, J. Kawasaki, J. Yamaguchi, *Appl. Surf. Sci.* **255**, 1617 (2008).

[11] M. L. Yu, *Nucl. Instrum. Methods Phys. Res.* **B 18**, 542, (1987).

[12] D. Takamatsu, Y. Koyama, Y. Orikasa, S. Mori, T. Nakatsutsumi, T. Hirano, H. Tanida, H. Arai, Y. Uchimoto, Z. Ogumi, *Angew. Chem., Int. Ed.* **51**, 11597 (2012).

査読コメント

査読者 1. 阿部芳巳（三菱化学科学技術研究センター）

本投稿論文は，FIB と TOF-SIMS を複合した新奇な装置を利用してリチウムイオン二次電池の正極材料として有用な $LiCoO_2$ の表面劣化を議論しており，実用材料の表面分析事例として JSA に掲載する価値が高いと考えます．

［査読者 1-1］

$LiCoO_2$, CoO, Co_3O_4 の 3 つの市販試薬を“ standard materials **”として利用しています．一般に，化合物の表面組成はバルク組成から乖離することがありますが，本論文で使用した試薬の表面が想定通りの化学組成であることをどやって確認したのでしょうか？化学種を議論するための参照として使うのであれば, 参照として適切であることを示す必要があり，それがないと説得性に欠けます．また，**Fig. 2 **をみると，**Na**，**K** などのアルカリや塩素などの汚染元素が検出されていますが，その共存の影響については検討したのでしょうか？**

［著者］

使用した試薬は市販の「試薬」であり厳密に管理された standard material **ではありません．また表面の組成がバルク組成と一致するかは確認できておりません．しかし，バルクの化学組成が異なるものの表面を測定して違いが見られたため，化学組成により発生する二次イオンの種類，あるいは強度比が異なるということがわかります．実試料において深さ方向に測定を行うと二次イオンの強度比が変化していくことも確認できたため，今後，より管理された標準試料を使用することにより，より厳密に区別を付けることが可能であると示唆されます．**

アルカリ金属・塩素等のコンタミネーションとの共存の影響につきましては厳密には検討できておりません．しかし，アルカリ金属・塩素等のコンタミネーションは，二次イオンマッピングで見ますと粒子全体でなく，スポット上に分布していることがわかります(次図参照)．このことから粒子全体を覆っていることはなく面分析においては影響が少ないと思われます．

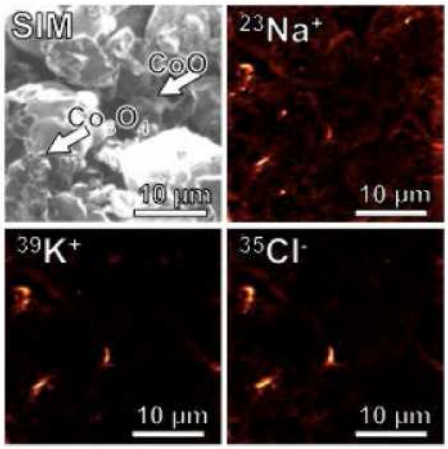

［査読者 1-2]

3.1 節で Na, K, F and Cl **は** In **基板由来である可能性を追記していますが，査読コメント[査読者** 1-1] **への回答では“粒子全体ではなく，スポット上に分布している”と記述しており，両者の記述は整合しているでしょうか？もし，アルカリやハロゲンが試**

料由来ではなく，In 基板由来であるとすれば，Na や Cl と In との分布状態の同期が認められるはずですので, 回答に示したイオン像に In のイオン像データを追加して示していただけると説得力が増すと思います.

［著者］

汚染元素は粒子上ではスポット上で存在しており，また，インジウム基板からも汚染元素が検出されております．前回の図では汚染元素は粒子上のコンタミネーションでありスポット状に分布しているものを出しました．一方，インジウム基板からの寄与も多く見られます.

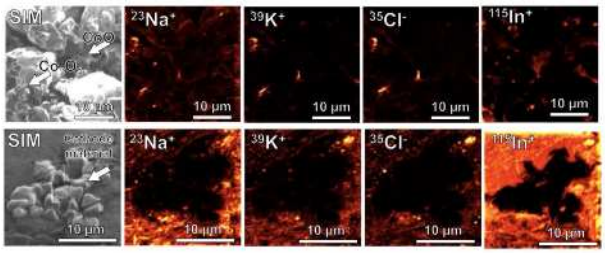

汚染元素の分布形状：(上)粒子の上にスポット状 (下)インジウム基板上

以下の記載を変更しました.

変更前：The contaminants, Na, K, F, and Cl were detected in all of the reagents, and may be due to the indium substrate.

変更後：The contaminants, Na, K, F, and Cl were detected in all of the reagents. These contaminations are distributed on the reagent grains as spot and on the indium substrate.

［査読者 1-3］

正極材は，大気下で電極から剥がしてインジウムに埋め込んだと記載されています．短時間であっても大気に曝露すれば，試料表面の変質が避けられないと思いますが，その影響については検討したのでしょうか？本論文が正極材表面の劣化の現象を正しく捕えているか否か判断する上で，大気暴露による影響が懸念されます.

［著者］

一般的に負極に対して正極は満充電でない限り大気の影響が少ないとされております．それは負極の標準電極電位が-2.9 V に対してコバルト酸リチウムは＋0.9 V でこれは銀以上白金以下であることから上記のようにいわれております（酸性溶液中において銀以上白金以下の安定性を示すということです).

また，電解液につけただけのもの(no aging)と比較し，no aging の深さ方向分析から，LiF が少ないことがわかります．大気暴露において電解液と水蒸気が反応すると HF が発生し，これが表面に作用し LiF を生成することがわかっております（電解液中に水分を含むと劣化が進む). この LiF が少ないということは，この試料準備手順において，大気暴露の影響が少ないということが言えます.

［査読者 1-4］

査読コメント[査読者 1-3]への回答として，2.2 節の最後に The influence of...was insignificant...の一文を追記していますが，was insignificant と断定した根拠が何も示されていません．回答に述べたような一般論を，出典を明記して引用するなどして，insignificant と考えた根拠を示す必要があると考えます.

［著者］

下記のように記載いたしました.

In general, cathode material of Li-ion battery that which is not full charge is stable than anode material. Because of the standard electrode potential (E_0) of $LiCoO_2$ is ~0.9 V [9]. The value indicates that $LiCoO_2$ is more stable than Ag, more unstable than Pt in acid solution.

［査読者 1-5］

また，3.3 節の 3 番目の段落の最後に and also confirms that the effect of exposure to the atmosphere was small の記述を追記していますが，何故 confirm されるのか，根拠となる ref などを示す必要があると思います.

［著者］

水分と反応して電解質である $LiPF_6$ が分解し，フッ化水素が発生することにより電極表面にフッ化リチウムが生成して表面が変質するという文献を引用いたしました.

［査読者 1-6］

回答では“正極は満充電でない限り大気の影響が少ない”という一般論を引用していますが，分析した試料は満充電でエージングテストしたと記述されています．大気下で電極から剥がす前に放電させたという理解でよいでしょうか？

［著者］

電池を解体する前に 70%程度に放電させております.

［査読者 1-7］

本論文では，マススペクトルの変化を正極材表面の劣化に結び付けて議論されています．劣化させていないブランク試料（aging test 0 時間）やより長時間劣化させた試料（aging test > 2 日）との対比があると, 導出された結論に説得性が増すと思いますが, ブランク試料などの分析結果はないのでしょうか？

［著者］

電解液につけただけのもの(no aging)と組み立てただけの試料(no soak)の分析結果を記載いたしました．また，その記載過程で新しい論文を引用いたしました.

［査読者 1-8］

本装置の面内での空間分解能はどれくらいでしょうか？その記述がないと，最後の結論の“less than 200nm”の根拠がわかりません.

［著者］

本測定における 1 ピクセルのサイズは 80 nm 四方です．これは本装置の最高空間分解能(40 nm, ref.10)より大きく，ビーム径に対してピクセルサイズが大きいことが示唆されます．このことより，ピクセルサイズ＝空間分解能に値します．しかし，物質中に含まれる元素の濃集具合により，実効空間分解能は変わります．Fig. 6 の全二次イオン強度プロファイルより，エッジ効果が 200 nm と見積もられ，$^{59}Co^+$ も全二次イオン強度プロファイルと同様の挙動を示します. このことからエッジ効果に $^{59}Co^+$の濃度変化が埋もれてしまい，見えなくなっていることが示唆されます．よって 200 nm と記載いたしました.

本文にも同様の記載をいたしました.

［査読者 1-9］

独自に開発された本装置では，細線化された Ga イオンを二次イオンの励起源に利用していますが，その照射ダメージについて検討しているでしょうか？つまり，今回使用した条件で Ga イオンを照射したときの二次イオン強度の経時的変化（ドーズプロファイル）について，検討しているでしょうか？そうした検討を踏まえて測定条件を設定していることを示せた方が測定データの信頼性が増すと考えられます.

［著者］

ドーズプロファイルは測定しておりません. また，分析条件の設定も，ドーズ量に関しては検討しておりません(おもに二次イオンマッピング時の元素分布が見えるような条件で測定しております). しかし，試料測定時と同様な分析条件で測定した試薬の二次イオンスペクトルと，論文記載の条件で分析を行った試薬の二次イオンスペクトルに大きな変化が見られないことから，ドーズ量に対しての二次イオンの強度変化は本分析条件においては影響が少ないと思われます.

［査読者 1-10］

査読コメント[査読者 1-8]への回答として，2.1 節の最後に The spatial resolution..., and corresponded to the grain size of each reagent.の一文を追記していますが，空間分解能がそれぞれの試薬のグレインサイズに対応するという記述の意味が分かりません．例えば，400nm サイズの粒子を測定した場合に，一次イオンのビーム径や画素サイズが粒子サイズよりも十分小さければ, 空間分解できるサイズは 400nm とは

限らずもっと小さくなるのではないでしょうか？（素朴な疑問です）

［著者］

画素の大きさに相当した(あるいはそれ以下の大きさの)ビーム径で測定を行えば，空間分解能はそれに相当してあがります．今回の場合，試薬によっては粒子径が大きく，空間分解能をあげても試薬の特徴が把握できづらいため，試薬の粒子径によっては相対的に低空間分解能で測定しております．

［査読者 1-11］

3.3 節の 4 番目の段落で，表面の CoO_2^-/Co^+強度比は内部に比べて高いと記述していますが，Fig. 8 のデータを拾う限り，当該強度比は表面の方が低いです．確認をお願いします．

［著者］

図中の強度を表す数字はその図内の最大強度を表しております(コントラスト等見やすいよう調整しておりますので図同士の比較をしやすいように記載いたしました)．Co につきましては最大強度が粒子のエッジの部分から観察され，粒子全体ではそこまで強度が出ておりません．下記の図を添付いたします．

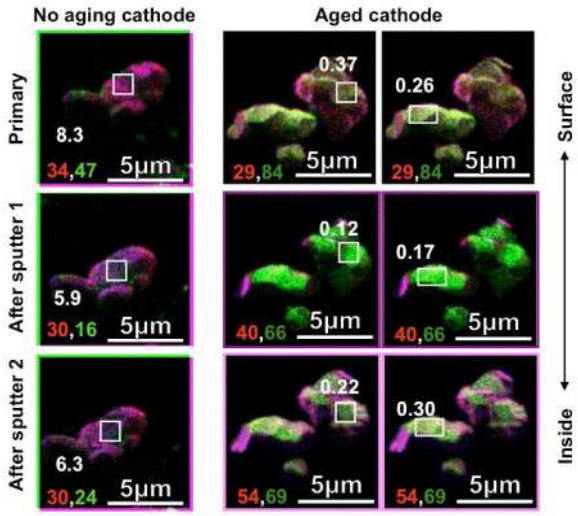

$^{59}Co^+$を緑，$^{75}CoO^-$を青，$^{91}CoO_2^-$を赤で表示した二次イオンマッピング結果．左下の添え字は画面内での最大強度を示す．赤：$^{91}CoO_2^-$，緑：$^{59}Co^+$．画面内の白抜きの数字は図内に四角で示されたエリアの $^{91}CoO_2^-/^{59}Co^+$の値である．

また，aged cathode の同様の処理をした結果を示します．この図で見ますと最表面は $^{91}CoO_2^-$と $^{59}Co^+$がともに検出されており，掘り進めるうちに相対的に $^{59}Co^+$の強度が高くなった後，内部では $^{91}CoO_2^-$の強度が高くなるということがわかります．このことから最表面には CoO・Co_3O_4 の両方が存在しており，その後，CoO 相に変わり，最終的には $LiCoO_2$ になっていると考えられます．

ただし，この方法では $^{59}Co^+$のスペクトルに $^{59}Li_3F_2^+$の裾が重なっている場合があり，特にフッ化リチウムの存在する aged cathode の表面では定量的な議論をするためにはより工夫が必要となります．

査読者 2．中村　誠（富士通研究所）

［査読者 2-1］

結局 $LiCoO_2$ の表面が，CoO や Co_3O_4 になるからダメと言っているように見えたのですが，もしそうなら，そうならないためにはどうすべきなのか？根本的に劣化は仕方がないことなのかを明示するようがいいと思います．要は書き出しに対して結論が弱いように思います．電極の劣化が重要であるということとエイジングで表面が変わるところはわかるのですがそれが劣化につながっているのかを示して，結論にするほうがいいと思います．表面が CoO_2 や Co_3O_4 になるから特性が劣化し，それをうまく評価するのに，TOF-SIMS が最も適している(他の方法では評価が難しい)といった結論でもいいと思います．

［著者］

本論文の趣旨は化合物が二次イオンマッピングにより識別できることなので，それに対応してイントロダクションを書き換えました．

［査読者 2-2］

Surface analysis で今回の FIB のビーム径，ラスタエリアに関して記載した方がいいと思います．また，「300 pA in DC mode」というのは SIMS 屋さんにはわかるかもしれませんが電子分光屋さんには何のことかわかりませんので少し説明してください．

［著者］

ビーム径についての記載を Under these analytical conditions, the beam diameter was considered to be ~ several tens of nm.と追記いたしました.

また，ラスタエリアにつきましては試料ごとに異なるため，それぞれの試料の結果に足しました.

300 pA in DC mode を The beam current of the FIB was approximately 300 pA.と修正いたしました.

［査読者 2-3］

Depth analysis の文がごちゃごちゃしていてわかり辛いのでフローチャート的に図示した方がわかりやすいと思います．またこの条件でどのくらいの領域がどのくらい掘れているのかも記した方がいいと思います.

［著者］

フローチャートを追加いたしました.

また，スパッタによって掘れる深さをスパッタ収率計算ソフトを用い計算した結果を記載いたしました.

［査読者 2-4］

アブストラクトと Results and discussion，Conclusion で 200 nm 以下と出てきますがどこからこの数字が出てきたのか不明瞭です．根拠を明示してください.

［著者］

Fig. 6 より edge effect が~200 nm と見積もられ，edge effect に隠れて判別できないため，less than 200 nm と記載しております．全体的に空間分解能・深さ分析の時のスパッタされた深さについての記載を増やしました.

［査読者 2-5］

Fig. 3 の倍率が違う理由はなんでしょうか？

［著者］

試薬の分析においてそれぞれのイメージの倍率が異なるのは，試薬の粒子の大きさがそれぞれ異なるため，その大きさに適した倍率で測定しているためです.